AIMS Energy, 13(4): 901–921.
DOI: 10.3934/energy.2025033
Received: 30 April 2025
Revised: 02 July 2025
Accepted: 29 July 2025
Published: 12 August 2025

https://www.aimspress.com/journal/energy

Research article

Composite sorbents "calcium chloride inside alumina and carbon mesopores" for thermochemical energy storage

Yuri I. Aristov, Mikhail M. Tokarev, Alexandra D. Grekova, Marina V. Solovyeva and Larisa G. Gordeeva*

Boreskov Institute of Catalysis, Pr. Lavrentieva 5, Novosibirsk, 630090 Russia

* **Correspondence:** Email: gordeeva@catalysis.ru; Tel: +738332699454.

Abstract: Thermochemical energy storage is an emerging technology aiming to mitigate the mismatch between heat supply and demand. Adsorption method, which belongs to the wider class of thermochemical energy storage, is a promising solution for storage of low-temperature heat (below 100 °C). Designing efficient energy storage units requires the appropriate choice of the working pair. In this article, we address the properties of composite sorbents "$CaCl_2$ inside alumina and carbon mesopores", two commercial matrices with similar pore structure, but very different chemical nature and hydrophilicity. Despite this, water sorption equilibrium for both composites are very similar; the composites' sorption properties are influenced more by the confined salt and the matrix' porous structure than by its chemical nature. This finding provides deeper insight into the adsorption mechanisms and can guide designing new advanced composites "salt in a porous matrix" for various applications. High heat storage density (1.1–1.3 GJ/m^3), low regeneration temperature (60–100 °C), high heat release temperature (up to 60–80 °C), good hydrothermal stability, and commercial availability of the components make the new $CaCl_2$/Alumina composite very competitive with other materials for thermochemical energy storage.

Keywords: thermochemical energy storage; salt hydration; composite sorbents; $CaCl_2$/Alumina; $CaCl_2$/carbon Sibunit; water sorption

Abbreviations: CSPM: composite "salt in porous matrix"; HSC: heat storage capacity; TCES: thermochemical energy storage; BET: Brunauer-Emmett-Teller; BJH: Barrett-Joyner-Halenda; NSA: normalized surface area

Nomenclature: C: content, wt.%; D: diffusivity, m^2/s; d: pore size, nm; E_a: activation energy, J/mol; ΔH: enthalpy, J/mol; ΔF: adsorption potential, J/mol; I: specific heat of immersion, J/m^2; k: rate constant, s^{-1}; l: grain size, mm; m: mass, g; N: mole ratio, mol_H_2O/mol_$CaCl_2$; P: pressure, mbar; $P_0(T)$: saturated vapor pressure at temperature T, mbar; Q: heat storage capacity, J/g; Q_v: volumetric heat storage capacity, J/m^3; R: universal gas constant, J/(mol·K); S_{sp}: specific surface area, m^2/g; T: temperature, °C, K; t: time, s; w: uptake, g/g; V_p: specific pore volume, cm^3/g; A, B, n, Z: fitting parameters

Subscripts/superscripts: 0: saturated; ∝: infinite; a: ambient; ad: adsorbent; av: average; c: composite; d: desorption; e: empty; is: isosteric; m: matrix; p: pore; r: rejection; s: salt; sol: solution; t: total

Greek symbols: ρ: density, g/cm^3; ε: porosity; χ: tortuosity; δ: thickness, m; τ: characteristic time, s

1. Introduction

The development of low- and zero-carbon energy systems is a strategic goal of the global energy policies, which requires the effective utilization of renewable energy sources. Thermochemical storage of solar or waste heat can mitigate the mismatch between the heat supply and demand, which is one of the major factors hindering their use [1]. Among methods for thermal energy storage, namely as sensible, latent, and chemical heat, the thermochemical method offers important benefits: Larger Heat Storage Capacity (HSC) and negligible heat losses during the storage phase. ThermoChemical Energy Storage (TCES) involves a reversible endothermal/exothermal reaction driven by a thermal energy source, e.g., solar or waste heat, and recover it when needed [2]. The diversity of the reactions applicable for TCES offers the possibility to vary the temperature level of the heat storage/release in a wide range (25–1000 °C) [3]. Among the many reactions for TCES, decomposition/formation of metal hydrides are characterized by high energy storage capacity up to 4200 kJ/kg (CaH_2) and flexibility to operate in different environmental conditions by varying the alloy composition to cover a wide range of operating temperature (from ambient to 1000 °C) and hydrogen pressure (from 0.001 bar to several hundred bars). Low temperature hydrides such as $NaAlH_4$ and $TiMn_{1.5}H_{2.5}$ possess moderate energy storage capacity below 1000 kJ/kg [4,5]. Low thermal conductivity of the metal hydrates is a crucial factor limiting their practical application. Metal carbonates are another class of materials that have attracted interest for TCES due to quite high energy storage capacity up to 1657 kJ/kg ($CaCO_3$) and economic attractiveness [6]. They are mostly intended for middle (100–300 °C) and high temperature (>300 °C) heat storage. Slow decomposition kinetics and reduction in the cycle uptake capacity are their drawbacks, which can be partially overcome by doping carbonates with additives. Both metal hydrides and carbonates can be applicable only for close TCES systems, in the absence of contact of reagent with the atmosphere.

Low temperature heat (below 100 °C) accounts for 63% of waste heat streams from electricity generation, transportation, industry, and domestic sectors [7–9]. For storing this low-grade heat, the TCES method, which involves a reversible process of water adsorption or hydration/dehydration of hygroscopic salts (S)

$$S+nH_2O(g) \Leftrightarrow S\cdot nH_2O + Q \quad (1)$$

is a promising route (Figure 1a). TCES includes two stages, namely the heat storage (charging), and the heat release (discharging). During the charging stage, the heat to be stored is used to carry out endothermic dehydration of salt hydrates $S{\cdot}nH_2O$ to form anhydrous salt and water vapor. Then, when heating is required, discharging stage occurs, and the stored energy is released during the exothermic reaction of the salt with water vapor [2,7]. Thus, TCES based on the salt hydration or adsorption involves a solid-gas reaction.

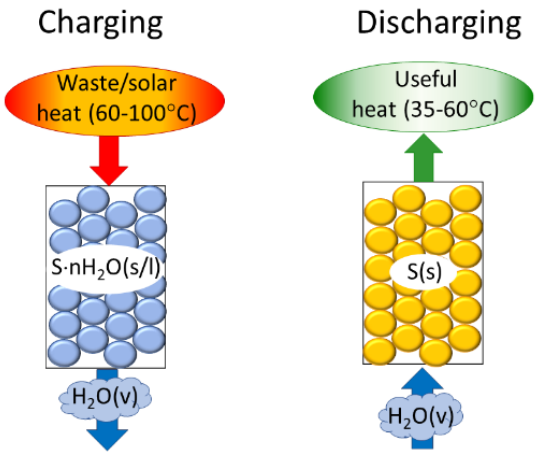

(a)

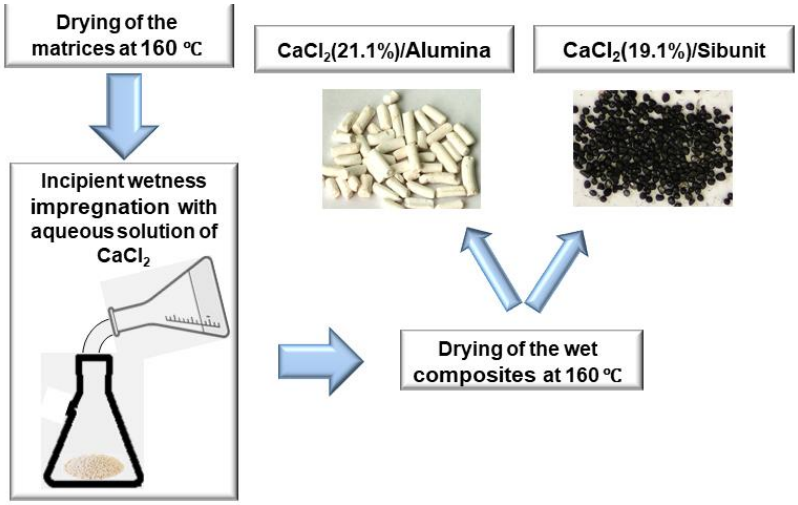

(b)

Figure 1. (a) Scheme of TCES based on the salt hydration; (b) Scheme of the composites' preparation.

Designing efficient TCES units requires the appropriate choice of a chemical reaction or an adsorbent, the properties of which have a significant impact on the performance indexes of TCES units [10]. However, the practical application of bulk salt hydrates for TCES is hindered by their deliquescence due to the water absorption, aggregation of salt particles in hydration/dehydration cycles,

and low thermal conductivity of salts, which result in poor hydration dynamics and low specific power of TCES units [7]. Several types of solid porous adsorbents have been proposed for TCES [11], such as crystalline aluminophosphates, metal-substituted aluminophosphates (AlPOs, MeAPOs) [12,13], and metal-organic frameworks (MOFs) [14,15]. However, the practical application of these materials for TCES is challenging because of high cost and poor commercial availability of these adsorbents.

A family of Composite materials "Salt in a Porous Matrix" (CSPM) was invented [16] and studied for TCES [17–20], as well as other applications such as maintaining relative humidity [21], shifting chemical equilibrium [22], etc. CSPM are two-component materials, which consist of a porous host matrix and a hygroscopic salt confined to the matrix pores. CSPMs take an intermediate position between common porous adsorbents and pure hygroscopic salts and can be organized in a way to combine the best features of both components.

Since salt is the main water sorbing component, the adsorption and energy storage capacities of CSPMs grow with an increase in the salt content [17,19]. The porous matrix is also of paramount importance as it contributes to heat and mass transfer in the adsorbent particles. Moreover, the porous structure of the matrix greatly affects the sorption equilibrium of the confined salt, which enables tuning the composite' properties by introducing the salt into pores of a certain size [17,19–25]. To the best of our knowledge, little is known on the influence of another important characteristic of the matrix, namely its chemical nature, which can be attributed to the complexity of finding the matrices of different chemical nature with the same porous structure.

In this article, two commercial mesoporous adsorbents with very similar porous structure, but completely different chemical nature and affinity to water, namely activated alumina and carbon Sibunit [26], were used as host matrices for $CaCl_2$. This enables us to gain insight into the influence of the chemical nature of the matrix on adsorption properties of the composites.

During the formation of solid $CaCl_2$ hydrates and aqueous solution, a large amount of heat is released [16,19,20,23] that promotes high energy storage capacity of $CaCl_2$-based CSPMs. $CaCl_2$ was introduced into other porous matrices (silica gel, zeolites, vermiculite, microporous carbons, MOFs, clays, SBA-15, etc.) [16,18,19]. However, only a few studies were devoted to $CaCl_2$-composites based on activated alumina [20,27] and none to composites based on a mesoporous carbon, such as Sibunit. Both matrices have very good structure stability and high strength, which is an important parameter because the composites must remain intact during numerous hydration/dehydration cycles. Thus, the commercially available active alumina has a crush strength of 16 kg, which is much higher than that for silica gels (3.6–9 kg) [28]. Relatively high bulk density (910 kg/m^3 for alumina as compared with 415 kg/m^3 for silica gel and 130 kg/m^3 for expanded vermiculite) is also profitable for energy-related applications as promotes a high volumetric energy storage capacity [29]. Thermal conductivity of monolithic and pelletized alumina equal to 23–28 and 0.28 W/m/K, respectively [29,30], is higher than that for $CaCl_2$ pellets (0.11–0.15 W/m/K) [31], which can contribute to fast sorption dynamics on the composite. Finally, it is worthy to note that both matrices and salt are commercially available and cheap (the cost of active alumina and $CaCl_2$ is 1.5–5 and 2–4 USD/kg, respectively). All these properties are beneficial for practical implementation of TCES using these composites.

The equilibrium of the water vapor adsorption on composites $CaCl_2$/Alumina and $CaCl_2$/Sibunit was studied and compared. The novelty of this study lies in revealing the effect of the matrix chemical nature on the water adsorption equilibrium of the composites, which become possible due to the use of these two matrices with similar porous structure but completely different chemical composition and hydrophilicity. The water sorption kinetics was studied for the $CaCl_2$/Alumina composite; its

hydrothermal stability was tested for the first time under 200 sorption-desorption cycles. Based on the equilibrium sorption data, the heat storage capacity, the temperatures of the composite regeneration, and the heat release were evaluated, and the effect of the operating conditions on the TCES performance was analyzed. The results showed a high potential of the composites for TCES.

2. Material and methods

2.1. Composite synthesis and characterization

Commercial alumina A1 (Angarsk Oil Refinery) and carbonaceous material Sibunit (Institute for Problems of Hydrocarbon Processing SB RAS) were used as host matrices for $CaCl_2$ (purity > 99%, Aldrich). The composites were prepared by an incipient wetness impregnation of the matrix's grains with an aqueous solution of $CaCl_2$ (30 wt. %) (Figure 1b). Before impregnation, both matrices were dried at 150 °C for 10 h, and the $CaCl_2$ solution was added to the matrices dropwise. The solution volume V_{sol} was equal to pore volume of the matrix, $V_{sol} = V_p m_m$, where V_p is the specific pore volume and m_m is the mass of the matrix. The wet composites were maintained in a closed vessel for 1 day to achieve uniform salt distribution inside pores and then dried at 150 °C for 16 hours. The salt content C_s was determined by weight method from the difference of the masses m_c of the dried composite and m_m of the pristine matrix according to the following equation:

$$C_s = [(m_c - m_m)/m_c] \cdot 100\% \quad (2)$$

The composites based on alumina and carbon were C_s = 21.1 and 19.4 wt. %, respectively.

The specific surface area, pore volume, average pore size, and pore size distribution were measured by nitrogen adsorption at 77 °C using a Micromeritics ASAP 2040 Analyzer in the range of the relative pressures P/P_0 = 0.06–0.99 with a step of 0.015. Before testing, a sample was degassed at 200 °C for 12 h in vacuum. The specific surface area S_{sp} was obtained by the Brunauer-Emmett-Teller (BET) method. The specific pore volume V_p was determined at P/P_0 = 0.99 (adsorption branch). The pore size distribution was obtained using the Barrett-Joyner-Halenda (BJH) method applied to the desorption branch of the isotherms. The morphology of the composites was characterized with a scanning electron microscope Regulus 8230 (Hitachi, Tokyo, Japan) with cold field emission at an accelerating voltage of 2.5 kV and 4 kV. The immersion heat was measured by a calorimeter Tian-Calvet as described in more detail in the Supplementary Materials (Section 1) and Ref. [32]. The total heat storage capacity of the sample was measured by DSC analysis using a DSC 404 C Pegasus calorimeter (Netzsch). Before measurements, the calorimeter was calibrated using the melting point and thermal effects of metal standards In, Bi, Sn, and Zn (see Section 4 in the Supplementary Materials). A sample weighed 20 mg was placed into a standard aluminium crucible, saturated with water vapor until pore filling, hermetically sealed, and kept for 24 h. Before measurements, a small hole was made in the crucible lid, then the sample was placed in the calorimeter measuring cell and heated in helium flow to 320 °C at a rate of 5 K/min. The results obtained were processed using standard Proteus Analysis software. Three measurements were made, and the average value was calculated.

2.2. Water sorption equilibrium and kinetics

Isobars of water sorption were measured by the thermogravimetric method in the temperature range 25–150 °C and partial pressure of water vapor P = 9–50 mbar with a Rigaku Thermoflex unit. Before measurements, a sample was placed into the measuring cell and heated to 150 °C in the flow of dry air to reach anhydrous state. The typical mass of dry sample m_{ad} was 20–25 mg, which corresponded to approximately one layer of loose composite grains on the bottom of the measuring cell. Then, humid air with a given partial vapor pressure P was passed through the measuring cell, maintaining a constant temperature of the sample. The dependence of the sample mass on time was recorded until the weight became constant, giving the kinetics of water sorption and the final change in the sample mass $\Delta m_\infty(T, P)$ equal to the equilibrium water sorption. The specific water uptake was presented as $w(T, P) = m_{H2O}/m_{ad}$ or as number N of moles of adsorbed water related to 1 mole of the salt $N = (m_{H2O}/M_{H2O})/(m_{ad}C_s/M_s)$; here, M_{H2O} and M_s are molar masses of the water and the salt.

The water sorption kinetics were measured for the fractions of the composite with grain size of 0.6–0.7, 1.4–1.5, 2.4–2.6, and 4.4–4.5 mm. The supply rate of humid air was carefully chosen so that it did not affect the kinetics of water sorption. Thus, the sorption kinetics was determined by vapor transport through the outer grain surface or/and inside the grain (Section 3.2).

2.3. Hydrothermal stability

First, the sorbent sample (grain size 4.5 mm) was saturated with the water vapor in a flux of humid air at a relative pressure of water vapor P/P_0 = 0.70 and temperature of 20–25 °C until the equilibrium. Then, it was dried in a dry air flux at 150 °C. After every 5–10 cycles, sorbent fragments smaller than 0.5 mm in size, formed as a result of sorbent degradation, were sifted out and the weight loss was determined. The equilibrium water uptake on the sample after 10 adsorption/desorption cycles was measured at a *RH* of 70% at room temperature. The weight of the sample was measured each hour until it become constant. The equilibrium uptake was calculated from the increase in the sample weight.

3. Results and discussion

3.1. Material characterization

Alumina A1 is a mesoporous material with a wide pore size distribution (Figure 2a) ranged between 2 and 20 nm with the average pore size d_{av} = 6.0 nm. The specific surface area S_{sp} = 195 m^2/g and the total pore volume V_p = 0.70 cm^3/g (Table 1) are typical for activated alumina [33,34]. Impregnation with the salt reduces the pore volume to V_p = 0.47 $cm^3/g\_composite$. The pore size distribution for the composite remains non-uniform with the same shape as before salt impregnation (Figure 2a).

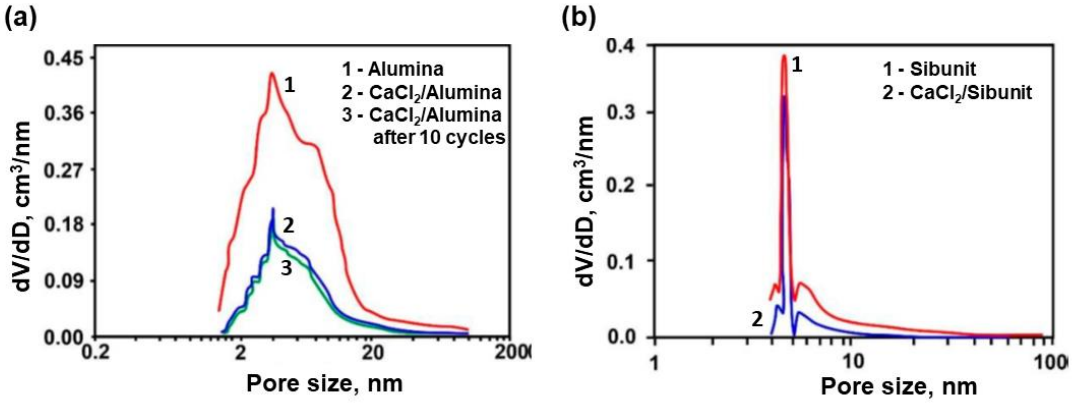

Figure 2. Pore size distribution of the studied matrices and composites.

Table 1. Salt content, specific surface area, total pore volume, and average pore size for the pristine matrices and appropriate composites.

	C_s, wt.%	S_{sp}, m^2/g	V_p, cm^3/g	$V_{p.th}$, cm^3/g	*NSA*	d_{av}, nm
Alumina	-	195	0.70	-	-	6.0
Sibunit	-	215	0.63	-	-	6.2
$CaCl_2$/Alumina	21.1	174	0.47	0.46	1.13	5.9
$CaCl_2$/Sibunit	19.4	156	0.33	0.42	0.9	5.8

The volume V_s occupied by salt related to 1 g of composite is equal to $V_s = C_s/100/\rho_s = 0.098$ cm^3; here, $\rho_s = 2.15$ g/cm^3 is the density of anhydrous $CaCl_2$. The theoretical pore volume available for N_2 molecules can be calculated assuming that $CaCl_2$ occupies internal pore space as $V_{p.th} = (V_p \cdot C_m) - V_s = (0.70\ cm^3/g \cdot 0.79\ g) - 0.098\ cm^3 = 0.46\ cm^3$, which is almost equal to the measured pore volume V_p of the composite. Moreover, the Normalized Surface Area NSA = S_{sp}(composite)/(1-C_s/100)·1/S_{sp}(matrix) is estimated as 1.13 (Table 1). NSA slightly exceeding 1 can be attributed to assembling the guest phase particles with the size comparable to the pore size of the matrix [35]. Indeed, the XRD pattern of $CaCl_2$/Alumina (Figure S1 in the Supplementary material) shows broad peaks at $2\theta \approx 20$ and 29–30°, which can be assigned to nano-dispersed $CaCl_2$ particles. The size of coherently scattering domains of $CaCl_2$ crystallites, estimated by X-ray diffraction and equal to 4–6 nm, is close to the average pore size of the alumina. SEM images of $CaCl_2$/Alumina composite (Figure S2 in the Supplementary material) show that it consists of rod-shaped primary alumina particles of about 0.1–0.3 μm length randomly bonded to each other (Figure S2). Some macropores are observed between the alumina particles. No bulky salt particle is observed on the external surface of alumina particles. These results confirm that $CaCl_2$ in the composite forms nanocrystals inside mesopores of the alumina.

The structure of the pristine carbon Sibunit is mesoporous and homogeneous with $d_{av} = 6.2$ nm, $S_{sp} = 215$ m^2/g, and $V_p = 0.63$ cm^3/g (Figure 2b). These texture characteristics are close to that for alumina. After impregnation with the salt, the pore volume decreases to $V_{p.c} = 0.33$ cm^3/g (Figure 2). Estimated the theoretical pore volume $V_{p.th} = 0.42$ cm^3 is somewhat larger than measured $V_p = 0.33$ cm^3/g. NSA is equal to 0.9. Thus, after impregnation, the pores become partially inaccessible to N_2. According to [35], it may indicate formation of the guest particles whose size is comparable to the pore diameter, deposited at least partially inside pores. SEM images of $CaCl_2$/Sibunit (Figure S2 in the Supplementary

material) show that the composite is composed of ensembles of round particles of 0.1–0.3 μm size connected to each other, forming some macropores between the particles. Again, no bulky salt particle is detected between these carbon particles. These results show that the salt particles are inside Sibunit pores near throat of narrow pores may partially block them [35]. This behavior is typical for matrices with small pores [17,24,36], such as the Sibunit. Indeed, no pores larger than 20–30 nm are detected in the pore size distribution (Figure 2b). Furthermore, the blocking may increase for hydrophobic matrices, which promotes formation of the droplets of the aqueous salt solution during drying the wet composite. Then, salt crystallization occurs from these droplets, which results in formation of the particles with the size closed to the pore size partially clogging the pores [37]. Similar behavior was observed for LiCl/alumina [38], LiCl/silica [39], and $CaCl_2$/MIL-101 composites [40].

The hydrophilicity of porous solids can be characterized by the heat of immersion in water (Table S1 in the Supplementary Materials). Indeed, the specific heat of alumina immersion in water $I = 0.290 \pm 0.006$ J/m^2 is one order of magnitude larger than $I = 0.0324 \pm 0.001$ J/m^2 for Sibunit. The alumina surface is highly hydrophilic due to the presence of active surface sites, including several types of hydroxyl groups (terminal -OH groups coordinated to a single Al^{3+} cation and bridging -OH groups, which links two or three Al^{3+} cation) [33]. These groups bear partial negative or positive charge and, consequently, have strong affinity to water [41]. For Sibunit, the heat of immersion in water coincides with the immersion heat (0.0322 J/m^2) of a non-porous graphite carbon black Grafon [42]. The Sibunit is produced by deposition of pyrolytic carbon on grains of graphitized carbon black followed by steam activation at high temperature of 700–1100 °C. Upon activation, narrow slit-like pores are formed, which give a sharp peak at 4–5 nm in the pore size distribution (Figure 2b). The surface of these pores mostly consists of highly hydrophobic basal faces of graphite-like carbon layers [26].

Thus, two commercial mesoporous matrices, activated alumina and carbon Sibunit, have close average pore size (ca. 6 nm), specific surface area (ca. 200 m^2/g), and total pore volume (0.63–0.70 cm^3/g), but very different chemical nature and hydrophilicity, they are used as host matrices for impregnating similar amounts of $CaCl_2$ (ca. 20 wt.%). Next, the water sorption on these composites is studied and compared, which enables identifying the effect of the matrix's chemical nature on the sorption properties of the composites.

3.2. Water vapor adsorption

For both composites, the sorption isobars are smooth curves, and the water uptake gradually decreases with increasing temperature (Figure 3); thus, the equilibrium sorption is bi-variant over the range of water uptake $w = 0–0.40$ g/g. Such type of water sorption equilibrium is typical of CSPMs with "narrow" pores, in which the hydrated salt can continuously change its composition as in an aqueous salt solution [17,19,24]. In "large" pores, the solid crystalline hydrates $CaCl_2 \cdot N H_2O$ ($N = 1/3$, 1, 2, and 4) are formed with a constant composition over a certain temperature range and a step-wise transition between them [17,19].

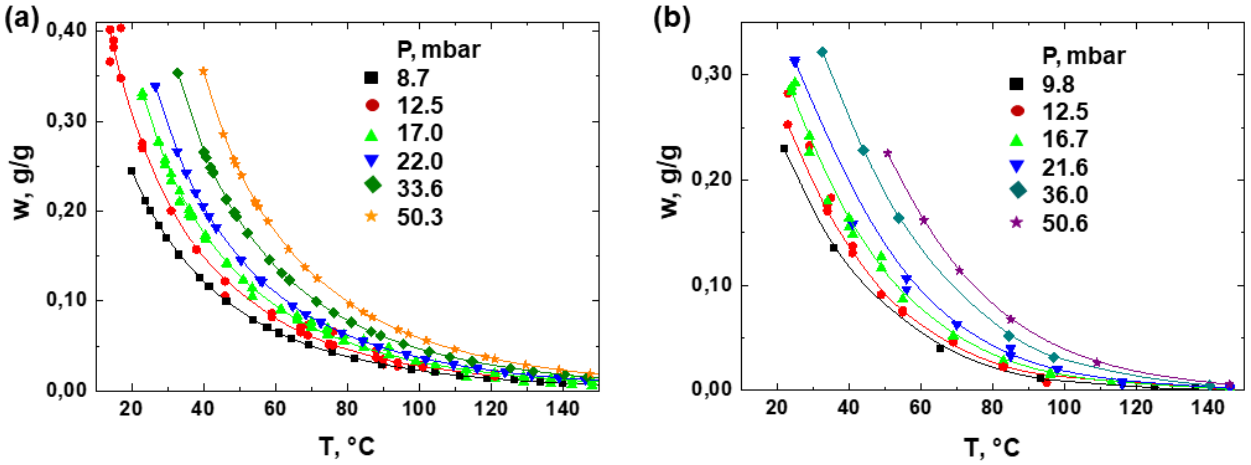

Figure 3. Isobars of water vapor sorption on the composites $CaCl_2$/Alumina (a) and $CaCl_2$/Sibunit (b).

Based on the experimental isobars, a set of sorption isosteres is plotted (Figure 4) and the isosteric heat $\Delta H_{is}(w)$ of water sorption is calculated according to the Clausius-Clapeiron equation

$$\ln(P_{H2O}) = \Delta H_{is}(w)/RT + C(w) \quad (3)$$

where $C(w)$ is a fitting coefficient. For both composites, the isosteric heat is almost the same in the uptake range $w = (0.07 – 0.24) \pm 0.005$ g/g or $N > 2$ mol/mol and tends to slightly decrease at increasing water content (Table 2). At a smaller w ($N < 2$ mol/mol), an increase in ΔH_{is} is observed, which can be attributed to the formation of the salt hydrate $CaCl_2 \cdot 2H_2O$ with stronger bonds between the water molecules and the salt ions. At large w-values, it approaches the evaporation heat for a bulk $CaCl_2$ aqueous solution [43].

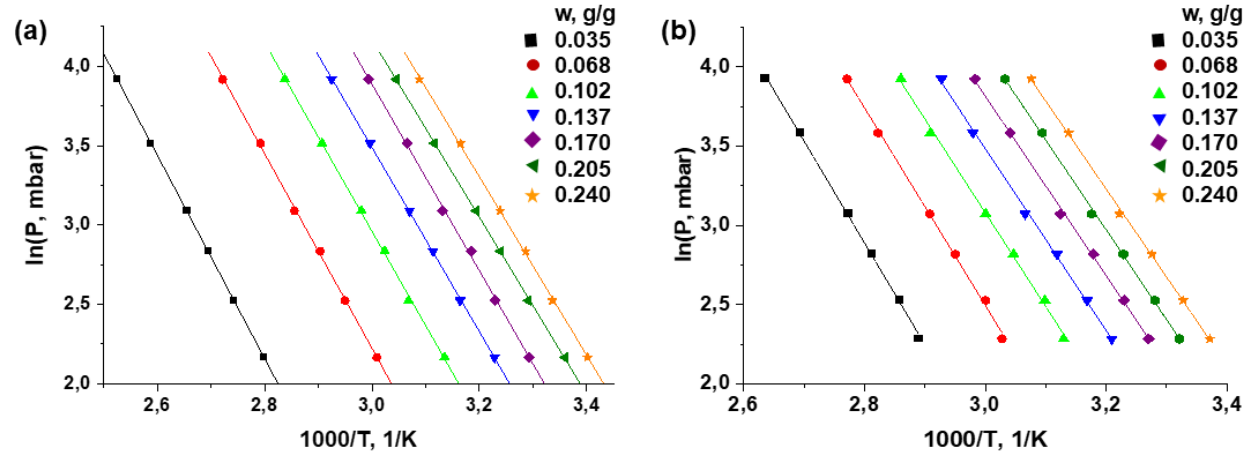

Figure 4. Isosteres of water sorption on the composites $CaCl_2$/Alumina (a) and $CaCl_2$/Sibunit (b).

Table 2. Isosteric sorption heat ΔHis (±1.0 kJ/mol) at various water uptakes *w* and *N*.

w, g/g	0.02	0.04	0.07	0.10	0.14	0.17	0.21	0.24
				$CaCl_2$/Alumina				
N, mol/mol	-	1.2	2.1	2.9	4.1	5.0	6.1	7.0
ΔH_{is}, kJ/mol		53.2	50.9	49.3	48.2	48.7	46.4	46.7
				$CaCl_2$/Sibunit				
N, mol/mol	0.6	1.3	2.2	3.2	4. 5	5.4	6.7	7.6
ΔH_{is}, kJ/mol	57.6	53.4	51.8	47.9	47.0	47.0	47.1	46.2

The set of these experimental data enables the water sorption properties of the composites involved to be thoroughly compared. For this purpose, the primary experimental data $w(P,T)$ are presented in a more universal form, e.g., as a function of water uptake on the Polanyi-Dubinin adsorption potential $\Delta F = -RT \cdot \ln[(P/P_0(T)]$, where R is the universal gas constant, T is the temperature, P is the water vapor pressure, and $P_0(T)$ is the saturated vapor pressure at temperature T (Figure S3 in the Supplementary Materials). All the experimental data (totally 154 readings), measured in a wide range of P = 8.7 – 50.3 mbar and T = 22–150 °C, well transform to one curve of water adsorption $w(\Delta F)$ for each the composite, which can be considered a universal characteristic curve of water adsorption.

In order to account for somewhat different salt content of 21.1 and 19.4 wt.% for $CaCl_2$/Alumina and $CaCl_2$/Sibunit, respectively, the adsorption data are related to the unit mass of the salt (Figure 5). This representation shows that in the small values of adsorption potential ΔF < 6.5 kJ/mol, the characteristic curves of the water sorption for both composites virtually coincide despite essential difference in the hydrophilicity of the matrices. This shows that the sorption properties of the composites, along with the salt' properties, depend more on the matrix porous structure than on its chemical nature (hydrophilicity). This may indicate that the sorbed water molecules interact more strongly with salt ions than with the adsorption sites of the matrix surface.

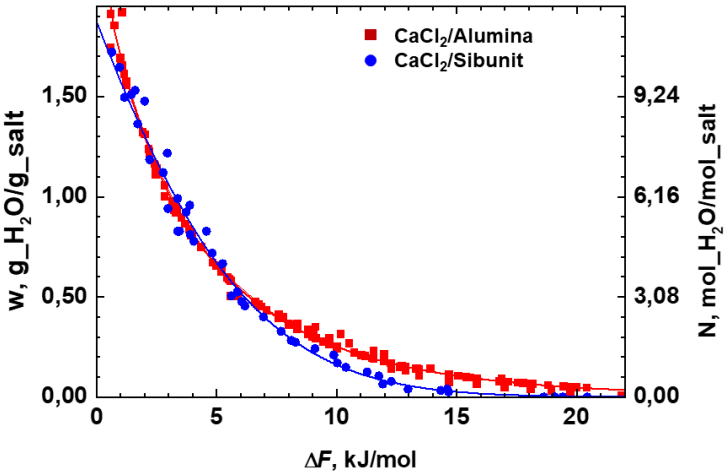

Figure 5. Characteristic curve $w(\Delta F)$ of water sorption related to the unit mass of the salt.

At ΔF > 6.5 kJ/mol, the $CaCl_2$/Sibunit based composite sorbs somewhat less water than $CaCl_2$/Alumina; the difference does not exceed 0.02 ± 0.01 g/g_c or 0.1 ± 0.05 g/g_{CaCl2} (Figure 5 and

Figure S3 in the Supplementary Materials). Probably at high ΔF-values, the chemical nature of the matrix starts affect the water adsorption. Indeed, at high adsorption potential (low relative pressure $P/P_0(T)$), the water molecules are adsorbed mainly on active adsorption sites of the matrix [17,24]. Accordingly, a higher affinity to water of the hydrophilic surface sites of alumina can cause slightly larger water uptake on $CaCl_2$/Alumina composite at $\Delta F > 6.5$ kJ/mol. Another reason for this deviation can be slight differences in the pore structure of alumina and Sibunit. Although the average pore sizes of the matrices are close, the pore size distribution for the Sibunit is much narrower. This matrix contains virtually no pores smaller than 4 nm, and the main contribution to its pore volume is made by pores with a size of ca. 5 nm (Figure 2b). Thus, it seems that the absence of small pores reduces the water sorption at large values of ΔF. Indeed, when calcium chloride is introduced into small pores, it begins to absorb water at a lower vapor pressure, i.e., greater ΔF [24].

A number of empirical and semi-empirical isotherms are used for description of water vapor adsorption on various adsorbents, including traditional Toth, Freundlich, Sips equations, and novel isotherms for multi-types adsorption [44,45]. The water sorption on the CSPMs involves several adsorption mechanisms, including the reaction between the salt and water resulting in the formation of the salt hydrates, the salt hydrates deliquescence, and further absorption of water vapor by the salt solution formed. Despite this, the Dubinin-Astakhov approach, although developed for the vapor adsorption on microporous adsorbents, is often employed as a model for analyzing the water, methanol, and ethanol sorption on CSPMs [46–48]. Indeed, the dependence $w(\Delta F)$ is well described by the common Dubinin-Astakhov equation [49], rewritten as:

$$w(\Delta F) = w_0 \cdot \exp[-(\Delta F/Z)^n], \quad (4)$$

(see Figure S3 in the Supplementary Materials), where w_0, Z and n are fitting parameters displayed in Table 3. Here, we apply the generally accepted assumption that the density of sorbed water does not depend on temperature over the narrow temperature range considered. It should be noted that, parameters Z and n are considered here as empirical, and Eq (4) is used only for the sake of comparison without delving into their physical meaning. Parameter w_0 can be considered the maximum water uptake. Thus, Eq (4) provides a fairly good approximation of the equilibrium data for predicting sorption equilibrium at any P and T values to compare the composites and estimate their energy storage capacity under the conditions of a specific TCES cycle.

Table 3. Fitting parameters w_0, Z, n of Eq (4) and coefficient of determination COD.

Matrix	w_0, g/g	Z, J/g·K	n	COD
Alumina	0.514 ± 0.007	3.49 ± 0.07	0.979 ± 0.01	0.997
Sibunit	0.407 ± 0.008	4.59 ± 0.09	1.17 ± 0.03	0.995

Thus, the adsorption properties of these CSPMs are more affected by the porous structure of the matrix; the effect of its chemical nature can likely appear only at high ΔF-values. This seems quite unexpected, because, for porous adsorbents, the chemical nature along with the porous structure are key-factors determining their adsorption properties. However, for CSPMs, the salt is the main absorbing component, and its chemical nature mainly influences the water sorption equilibrium. Furthermore, the porous structure of the matrix determines the size of the salt particles due to geometrical constrains. When salt is dispersed inside nano-pores of a few nanometers in size, its

properties become size dependent. Thus, the porous structure of the matrix may affect the adsorption equilibrium of CSPMs [17]. Therefore, the choice of expensive and exotic matrices, like MOFs and graphene oxide aerogel can be justified if some unusual sorption properties appear due to a strong and specific interaction between the salt and the matrix. Otherwise, cheaper and readily available matrices can be used, including mineral ones [20,50], such as expanded vermiculite [51], perlite [52], Wakkanai shale [53], attapulgite [12], pumice [54], and bentonite [55].

The detailed kinetic study of water adsorption has been performed for the composite $CaCl_2$/Alumina because activated alumina is a low-cost and readily available mesoporous material, which along with its adsorption properties, makes this composite more promising for practical large-scale application. Typical kinetic curves of water sorption $m(t)$ on the composite $CaCl_2$/Alumina (Figure 6a) turn into straight lines (Figure 6b) when plotted in the coordinates $\ln[1-\Delta m(t)/\Delta m_\infty)]$ vs. t. Here, $\Delta m(t)$ and Δm_∞ are the current and final mass change, respectively. This means that the uptake curves obey the first order equation

$$\Delta m(t) = \Delta m_\infty \cdot [1 - \exp(-k \cdot t)], \quad (5)$$

where k is the sorption rate constant.

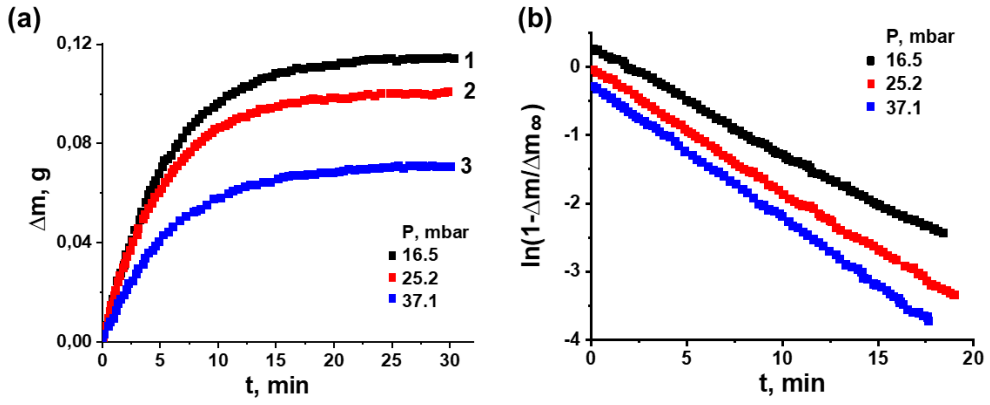

Figure 6. (a) Experimental curves of water sorption on the composite $CaCl_2$/Alumina and (b) their presentation by Eq (5), grain size l = 2 mm, T = 38 ºC.

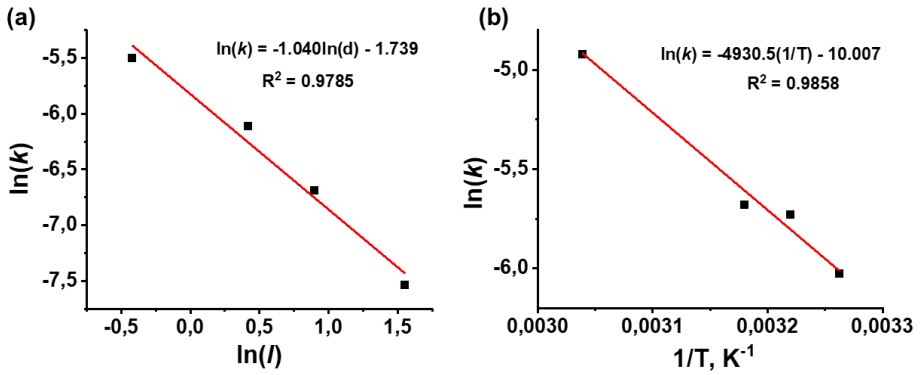

Figure 7. (a) Dependences of the sorption rate constant k on the grain size l and (b) on the reciprocal of the temperature $1/T$. P = 15.6 mbar (a, b), T = 38 °C (a), l = 2 mm.

The first order kinetic behavior (Eq (5)) is often observed in adsorption systems and can be attributed to the kinetic regime when the surface resistance controls the adsorption rate [56]. In this case, the kinetics is determined by vapor transport through the external grain surface, and the sorption rate related to the grain volume is proportional to the inverse grain size $1/l$. Indeed, the observed rate constant k increased for smaller grains as $k \sim 1/l$ (Figure 7a). For the composite $CaCl_2$/Alumina, this surface resistance can be caused by the formation of a salt solution in pores near the grain external surface. These pore spaces, filled with the solution, form a film at the grain surface and, as a result, water sorption kinetics can be controlled by the slow diffusion of water molecules through this film.

The sorption rate constant (or effective mass transfer rate constant) k can be expressed in terms of the effective water diffusivity D_{ef} in the solution film, the mass transfer surface related to the spherical grain volume $S/V = 6/l$, and the film thickness δ, $k = D_{ef} \cdot S/V/\delta$. If we assume a typical film thickness $\delta = 10^{-4}$ m, the effective water diffusivity D_{ef} can be estimated from the experimental rate constant as $D_{ef} = 4 \cdot 10^{-11}$ m^2/s. The obtained value is smaller by a factor of 30 than the water diffusivity D_b in bulk aqueous solutions of $CaCl_2$ equal to $1.2 \cdot 10^{-9}$ m^2/s [57]. First, water transport in the salt solution confined to the alumina pores slows down compared to the bulk solution because the space occupied by the alumina skeleton is inaccessible for water transport. The porosity of an alumina grain $\varepsilon = V_p/(V_p\text{-}1/\rho_{Al2O3}) = 0.74$ (here, $\rho_{Al2O3} = 3.99$ g/cm^3 is true density of Al_2O_3) reduces the diffusivity by a factor of 1.4. The diffusivity further decreases due to the tortuosity χ of the alumina pores, which accounts for the increased path length and the pore connectivity. Typically, the tortuosity factor is 2–4 [8]. Thus, the combined effect of porosity and tortuosity can reduce the effective water diffusivity $D_{ef} = D_b\varepsilon/\chi$ several times.

This stronger deceleration can be attributed to the slowing of water transport at the "vapor-solution" interphase boundaries. Indeed, due to capillary phenomena, solution domains inside pores can be interspersed with vapor domains. This can additionally slow the water transport, since the exit of a water molecule from the solution phase into the vapor phase may require overcoming the activation barrier [58].

The existence of such a barrier comes from the observed acceleration of water sorption with an increase in temperature from 30 to 55 °C. The temperature dependence of the rate constant plotted in the Arrhenius coordinates is a straight line (Figure 7b), which slope gives the activation energy E_a of water sorption equal to 45 ± 2 kJ/mol. This value is close to the heat of water sorption displayed in Table 3. The authors of [27] reported a smaller rate constant $9.6 \cdot 10^{-5}$ s^{-1} and a higher activation energy E_a = 66–69 kJ/mol for water sorption on a 15 wt.% $CaCl_2$/Alumina composite at 20 °C and 30% RH. However, the composite grain size was not reported, which does not enable a more detailed comparison.

Thus, these kinetic data may be useful to analyze open adsorption units for seasonal heat storage, air dehumidification, and regeneration of heat and moisture in ventilation systems, which utilize the composite $CaCl_2$/Alumina.

3.3. Evaluation of TCES cycle performance

TCES is one of the most promising applications of CSPMs based on activated aluminas [27,29,59,60]. These composites can be more in demand for open adsorption systems due to very good structure stability, high crush strength, and excellent hydrothermal stability (Section 3.4). The total heat storage capacity Q_t is estimated from the maximum mass of water desorbed and the average heat of sorption, $Q_t = \Delta w \Delta H_{is.av}/M_{H2O} = 1.3 \pm 0.05$ kJ/g_ads, where M_{H2O} is the molar weight of the water. The total

heat storage capacity is measured by DSC analysis $Q_{t.ex}$ = 1.23 ± 0.05 kJ/g_ads (Figure S4 in the Supplementary Materials), which is very close to the estimated Q_t - value. The average enthalpy of the water desorption obtained by DSC ΔH_{av} = 44.5 ± 0.7 kJ/mol_H_2O is somewhat lower than isosteric heat ΔH_{is} = 46.7–53.2 kJ/mol (Table 2) calculated from water adsorption isosters. This can be caused by a further decrease in the isosteric heat at water uptake w > 0.24 g/g and partial water desorption from the sample after making a hole in the lid before heating the sample. The obtained $Q_{t.ex}$-value is larger than the heat storage capacity Q_t = 576 J/g reported in [27], probably because the authors used the commercial alumina with a smaller pore volume of 0.25 cm^3/g. The total heat storage capacity of mesoporous γ-Al_2O_3 with a larger pore volume of 0.37–0.54 cm^3/g impregnated with $CaCl_2$ (15 wt.%) [20] is estimated as Q_t = 1.03 kJ/g. Considering here the bulk density of the composite equal to 1,090 kg/m^3, the volumetric heat storage density of the studied $CaCl_2$/Alumina composite is calculated as Q_v = 1.34 ± 0.05 GJ/m^3.

Another characteristic of the adsorbent important for TCES is charging temperature T_{ch}, which drives the sorbent regeneration. Figure 3a shows that the temperature needed for the complete removal of the sorbed water from $CaCl_2$/Alumina composite decreases at a lower partial pressure of water vapor but exceeds 150 °C even at P = 8.7 mbar. However, most of the sorbed water can be removed at T < 60–80 °C, which is available from simple solar collectors [61] or low-temperature waste heat [62]. Let us assume that the composite $CaCl_2$/Alumina is regenerated by ambient air with RH = 50% at ambient temperature of 30 °C (or at water vapor pressure P = 22 mbar) heated to T_{ch} = 60, 80, and 100 °C. Then, the specific mass of water remained adsorbed can be evaluated directly from the corresponding isobar in Figure 3a as 0.12, 0.07, and 0.04 g/g. This incomplete desorption leads to the heat storage capacity equal to 1.0, 1.1, and 1.2 kJ/g, which is slightly lower than Q_t = 1.3 ± 0.05 kJ/g, but remains encouraging (even at the low regeneration temperature 60 °C). Especially promising are values of the heat storage capacity related to a unit volume of the composite, 1.1, 1.2, and 1.3 GJ/m^3.

The heat release temperature T_{dis} is also of primary importance since, at this temperature, the stored heat is supplied to the consumers, and it must meet their needs. This can be roughly evaluated from the characteristic curve of water adsorption (Figure S3): If the adsorbent is regenerated at P = 22 mbar and T_{ch} = 100 °C, the sorbed water is removed from the adsorption sites with an affinity $\Delta F \leq -RT_{ch} \ln[P/P_0(T_{ch})]$ = 12.1 kJ/mol. At the heat release stage, these sites adsorb water vapor. If the ambient temperature T_{am} = 10 °C and RH = 50% (or water vapor pressure P = 6.2 mbar), these sites sorb water vapor if $\Delta F = -RT_{dis} \ln[P/P_0(T_{dis})] \leq 12.1$ kJ/mol. Then, the maximum T_{dis} can be estimated as 76 °C, providing the temperature lift (T_{dis}-T_{am}) up to 66 °C. At higher RH = 70% and vapor pressure P = 8.7 mbar, the maximum T_{dis} is higher and equals 82 °C, with the temperature lift up to 72 °C.

In modern houses, low temperature space heating systems such as floor heating are widely used, which can operate at supply temperatures below 40 °C. For domestic hot water production, temperatures of 60 °C are normally required to prevent growth of bacteria [63]. These space heating and hot water temperatures can be provided during the discharge phase of adsorption system operating with the studied $CaCl_2$/Alumina composite.

3.4. Hydrothermal stability

Hydrothermal stability at sorption/desorption cycles is a characteristic of adsorbents that is important for practical implementation of TCES, since the composites are subject to numerous adsorption/desorption cycles, particularly in short-term (daily) TCES. It turned out that the destruction

of the composite $CaCl_2$/Alumina does not exceed 0.004–0.005 wt.% per cycle, and its rate decreases at increasing number of cycles, so that after 200 cycles, the weight loss is less than 1% (Figure 8). The equilibrium water uptake on the composite after ten consequent sorption/desorption cycles is measured as 0.36 ± 0.01 g/g at RH = 70 ± 1%, which is similar to that for the as-prepared sample (0.37 ± 0.01 g/g). It is known that adsorption performance degradation usually occurs during the first adsorption/desorption cycles. Thus, the data obtained enables us to expect good durability of $CaCl_2$/Alumina composite upon further cycling.

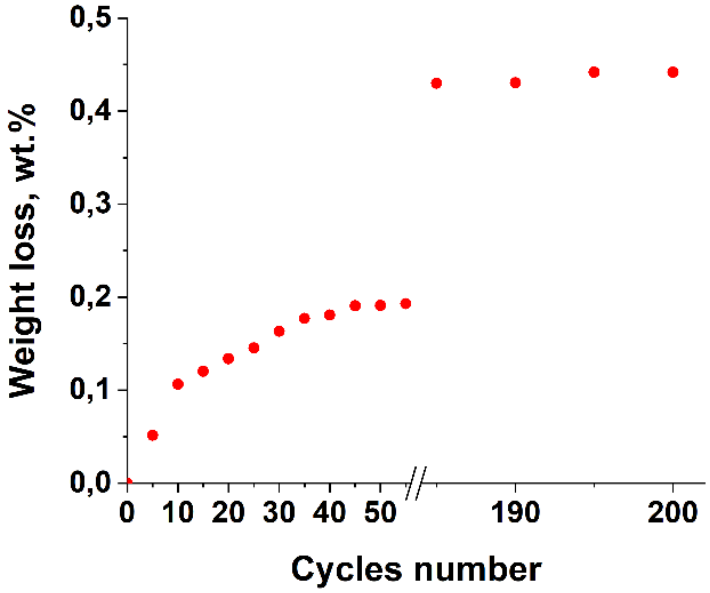

Figure 8. Weight loss of $CaCl_2$/Alumina composite vs. cycle number.

It should be noted that the salt deliquescence during water sorption, which results in its agglomeration during cycling and the deceleration of the water sorption/desorption, is a major challenge hindering the use of bulky salts for TCES. At a relative pressure of water vapor of 0.70, the equilibrium water uptake w = 0.37 g/g is lower than the composite' pore volume V_p = 0.47 cm^3/g. Accordingly, the formed salt solution is retained within the pores by capillary forces, which prevents salt agglomeration. Indeed, the pore size distribution of the composites before and after the cycles are similar (Figure 2a), which indirectly indicates that the salt distribution inside the alumina pores does not change. During cycling, the adsorbent is regenerated at a high temperature of 150 °C to almost dry state. During typical TCES cycles driven by solar collected by simple tube collectors, the regeneration temperature is lower (80–120 °C); thus, the hydrothermal stability of the composite is expected to be better.

Thus, due to a high energy storage capacity, low regeneration temperature, high released heat temperature, good hydrothermal stability, and readily available components at a reasonable price, the composite $CaCl_2$/Alumina can be very attractive for industrial implementation of TCES technology.

4. Conclusions

Our aim of this study was to study new composite sorbents "calcium chloride in mesoporous matrix" for TCES. Highly hygroscopic salt $CaCl_2$ was impregnated into two commercial mesoporous matrices, namely, activated alumina and carbon Sibunit, which have a fairly similar porous structure but differ greatly in chemical composition. The novelty of this study lies in revealing the effect of the matrix chemical nature on the water adsorption equilibrium of the composites. We show, for the first time, that despite the very different chemical nature and hydrophilicity of the matrices, the isobars and isosteric heat of water sorption appear to be very similar. Both composites possess di-variant water sorption equilibrium, indicating no formation of the crystalline hydrates $CaCl_2 \cdot NH_2O$. The isosteric heat of water sorption for both composites decreases from 53 ± 1.0 kJ/mol to 46 (±1.0 kJ/mol) at increasing water uptake from 0.04 to 0.24 g/g. This shows that the composite sorption properties are more influenced by the pore structure of the matrix than by its chemical nature, which can have some effect only at high values of adsorption potential. This finding provides deeper insight into the adsorption mechanisms and can guide designing new advanced composites "salt in a porous matrix" for various applications.

For the $CaCl_2$/Alumina composite, kinetics of the water sorption from a humid air flow is studied; the sorption rate constant is measured as a function of the size of composite grains (0.5–4.5 mm) and temperature (35–55 °C). The apparent activation energy is 45 kJ/mol. These equilibrium and kinetic data are used to analyze open TCES cycles. The new composite $CaCl_2$/Alumina possesses a good heat storage capacity (1.0–1.3 GJ/m^3), low regeneration temperature (60–100 °C), and high heat release temperature (up to 60–80 °C). The composite demonstrates a good hydrothermal stability with no significant change of the adsorption capacity during ten adsorption/desorption cycles. These properties, along with the wide availability of the components, make $CaCl_2$/Alumina very attractive for industrial implementation of TCES technology.

Use of AI tools declaration

The authors declare they have not used Artificial Intelligence (AI) tools in the creation of this article.

Acknowledgments

This work was supported by the Ministry of Science and Higher Education of the Russian Federation within the governmental order for the Boreskov Institute of Catalysis [project number FWUR-2024-0036]. Authors thank Mr. A. Sheshkovas for DSC measurements.

Conflict of interest

All authors declare no conflicts of interest in this paper.

Author contributions

Yu.I. Aristov: Conceptualization, Methodology, Writing—Original draft preparation, Reviewing and editing, Supervision; M.M. Tokarev: Investigation, Data curation; A.D. Grekova: Investigation, Visualization; M.V. Solovyeva: Investigation; L.G. Gordeeva: Visualization, Data curation; Writing—Reviewing and Editing, Project administration.

References

1. Wang R, Wang L, Wu J (2014) Adsorption refrigeration technology: Theory and application. Singapore: John Wiley & Sons, Singapore Pte. Ltd. Available from: https://www.wiley.com/en-us/Adsorption+Refrigeration+Technology%3A+Theory+and+Application-p-9781118197479.
2. Aydin D, Casey SP, Riffat S, et al. (2015) The latest advancements on thermochemical heat storage systems. *Renew Sustain Energy Rev* 41: 356–367. https://doi.org/10.1016/j.rser.2014.08.054
3. Deutsch M, Müller D, Aumeyr C, et al. (2016) Systematic search algorithm for potential thermochemical energy storage systems. *Appl Energy* 183: 113–120. https://doi.org/10.1016/j.apenergy.2016.08.142
4. Manickam K, Mistry P, Walker G, et al. (2019) Future perspectives of thermal energy storage with metal hydrides. *Int J Hydrogen Energy* 44: 7738–7745. https://doi.org/10.1016/j.ijhydene.2018.12.011
5. Milanese C, Jensen TR, Hauback BC, et al. (2019) Complex hydrides for energy storage. *Int J Hydrogen Energy* 44: 7860–7874. https://doi.org/10.1016/j.ijhydene.2018.11.208
6. Desage L, McCabe E, Vieira AP, et al. (2023) Thermochemical batteries using metal carbonates: A review of heat storage and extraction. *J Energy Storage* 71: 107901. https://doi.org/10.1016/j.est.2023.107901
7. Zhao Q, Lin J, Huang H, et al. (2021) Optimization of thermochemical energy storage systems based on hydrated salts: a review. *Energy Build* 244: 111035. https://doi.org/10.1016/j.enbuild.2021.111035
8. Miró L, Gasia J, Cabeza LF, (2016) Thermal energy storage (TES) for industrial waste heat (IWH) recovery: A review. *Appl Energy* 179, 284–301. https://doi.org/10.1016/j.apenergy.2016.06.147
9. Formann C, Muritala IK, Pardemann R, et al. (2016) Estimating the global waste heat potential. *Renew Sust Energ Rev* 57: 1568–1579. https://doi.org/10.1016/j.rser.2015.12.192
10. Aristov YI (2021) Adsorptive conversion of ultra-low temperature heat: Thermodynamic issues. *Energy* 236: 121892. https://doi.org/10.1016/j.energy.2021.121892
11. Henninger SK, Ernst SJ, Gordeeva L, et al. (2017) New materials for adsorption heat transformation and storage. *Renew Energy* 110: 59–68. https://doi.org/10.1016/j.renene.2016.08.041
12. Jänchen J, Ackermann D, Weiler E (2005) Calorimetric investigation on zeolites AlPO4's and $CaCl_2$ impregnated attapulgite for thermochemical storage of heat. *Thermochim Acta* 434: 37–41. https://doi.org/10.1016/j.tca.2005.01.009
13. Palomba V, Vasta S, Freni A (2017) Experimental testing of AQSOA FAM Z02/water adsorption system for heat and cold storage. *Appl Thermal Eng* 124: 967–974. https://doi.org/10.1016/j.applthermaleng.2017.06.085

14. Henninger SK, Jeremias F, Kummer H, et al. (2017) MOFs for use in adsorption heat pump processes. *Eur J Inorg Chem* 2012: 2625–2634. https://doi.org/10.1002/ejic.201101056
15. Elsayed A, Elsayed E, Al-Dadah R, et al. (2017) Thermal energy storage using metal-organic framework materials. *Appl Energy* 186: 509–519. https://doi.org/10.1016/j.apenergy.2016.03.113
16. Levitskii EA, Aristov YI, Tokarev MM, et al. (1996) "Chemical Heat Accumulators": A new approach to accumulating low potential heat. *Sol Energy Mater Sol Cells* 44: 219–235. https://doi.org/10.1016/0927-0248(96)00010-4
17. Gordeeva LG, Aristov YI, (2012) Composites "salt inside porous matrix" for adsorption heat transformation: a current state of the art and new trends. *Int J Low Carb Tech* 7: 288–302. https://doi.org/10.1093/ijlct/cts050
18. Tan B, Luo Y, Liang X, et al. (2019) Composite salt in MIL-101(Cr) with high water uptake and fast adsorption kinetics for adsorption heat pumps. *Microporous Mesoporous Mater* 286: 141–148. https://doi.org/10.1016/j.micromeso.2019.05.039
19. Aristov YI (2020) Nanocomposite Sorbents for Multiple Applications. *Jenny Stanford Publishing*. https://doi.org/10.1201/9781315156507
20. Ocvirk M, Ristic A, Logar NZ, et al. (2021) Synthesis of mesoporous γ-alumina support for water composite sorbents for low temperature sorption heat storage. *Energies* 14: 7809. https://doi.org/10.3390/en14227809
21. Glaznev I, Alekseev V, Salnikova I, et al. (2009) ARTIC-1: A new humidity buffer for showcases. *Stud Conserv* 54: 133–148. https://doi.org/10.1179/sic.2009.54.3.1
22. Gordeeva LG, Khassin AA, Chermashentseva GK, et al. (2012) New adsorbents of methanol for the intensification of methanol synthesis. *React Kinet Mech Cat* 105: 391–400. https://doi.org/10.1007/s11144-011-0379-z
23. Bu X, Wang L, Huang Y (2013) Effect of pore size on the performance of composite adsorbent. *Adsorption* 19: 929–935. https://doi.org/10.1007/s10450-013-9513-8
24. Ponomarenko IV, Glaznev IS, Gubar AV, et al. (2010) Synthesis and water sorption properties of a new composite "$CaCl_2$ confined to SBA-15 pores". *Microporou Mesoporou Mat* 129: 243–250. https://doi.org/10.1016/j.micromeso.2009.09.023
25. Zhou H, Zhang D (2022) Investigation on pH/temperature-manipulated hydrothermally reduced graphene oxide aerogel impregnated with $MgCl_2$ hydrates for low-temperature thermochemical heat storage. *Sol Energy Mater Sol Cells* 241: 111740. https://doi.org/10.1016/j.solmat.2022.111740
26. Ermakov YI, Surovikin VF, Plaksin GV, et al. (2087) New carbon material as support for catalysts. *React Kinet Cat Lett* 33: 435-440. https://doi.org/10.1007/bf02128102
27. Jabbari-Hichri A, Bennici S, Auroux A (2017) $CaCl_2$-containing composites as thermochemical heat storage materials. *Sol Energy Mater Sol Cells* 172: 177–185. https://doi.org/10.1016/j.solmat.2017.07.037
28. https://www.silicagelco.com/ (last accessed 26.08.204)
29. Zhang YN, Wang RZ, Li TX (2017) Experimental investigation on an open sorption thermal storage system for space heating. *Energy* 141: 2421–2433. https://doi.org/10.1016/J.Energy.2017.12.003
30. Parchovianský M, Galusek D, Švan čárek P, et al. (2014) Thermal behavior, electrical conductivity and microstructure of hot pressed Al_2O_3/SiC nanocomposites. *Ceram Int* 14: 14421–14429. https://doi.org/10.1016/j.ceramint.2014.06.038

31. Wang K, Wu JY, Wang RZ, et al. (2006) Effective thermal conductivity of expanded graphite-$CaCl_2$ composite adsorbent for chemical adsorption chillers. *Energ Convers Manage* 47: 1902–1912. https://doi.org/10.1016/j.enconman.2005.09.005
32. Pankratiev YD, Tanashev YY, Kulko EV, et al. (2006) Heat of wetting of aluminum hydroxide obtained by thermal activation of hydrargillite. *Rus J Phys Chem* 80: 1037–1043. https://doi.org/10.1134/S0036024406070077
33. Knoezenger H, Ratnasamy P (1978) Catalytic aluminas: Surface models and characterization of surface sites. *Catal Rev Sci Eng* 17: 31–69. https://doi.org/10.1080/03602457808080878
34. Desai R, Hussain M, Ruthven DM (1992) Adsorption of water vapor on activated alumina. I—Equilibrium behavior. *Canadian J Chem Eng* 70: 699–706. https://doi.org/10.1002/cjce.5450700412
35. Vradman L, Landau MV, Kantorovich D, et al. (2005) Evaluation of metal oxide phase assembling mode inside the nanotubular pores of mesostructured silica. *Microporou Mesoporou Mater* 79: 307–318. https://doi.org/10.1016/j.micromeso.2004.11.023
36. Cortés FB, Chejne F, Carrasco-Marín F, et al. (2012) Water sorption on silica- and zeolite-supported hygroscopic salts for cooling system applications. *Energy Convers Manag* 53: 219–223. https://doi.org/10.1016/j.enconman.2011.09.001
37. Neimark A, Kheifez LI, Fenelonov VB (1981) Theory of preparation of supported catalysts. *Ind Eng Chem Product Res Devel* 20: 439–450. https://doi.org/10.1021/i300003a006
38. Shkatulov A, Gordeeva LG, Girnik IS, et al. (2020) Novel adsorption method for moisture and heat recuperation in ventilation: Composites "LiCl/matrix" tailored for cold climate. *Energy* 201: 117595. https://doi.org/10.1016/j.energy.2020.117595
39. Gordeeva L, Freni A, Krieger T, et al. (2008) "Composites "Lithium Halides in Silica Gel Pores": Methanol Sorption Equilibrium". *Microporous Mesoporous Mater* 112: 254–261. https://doi.org/10.1016/j.micromeso.2007.09.040
40. Solovyeva MV, Krivosheeva IV, Gordeeva LG, et al. (2023) Salt confined in MIL-101(Cr)—tailoring the composite sorbents for efficient atmospheric water harvesting. *ChemSusChem* 16: e202300520. https://doi.org/10.1002/cssc.202300520
41. Ivanova AS (2012) Aluminium oxide and systems based on it: Properties and applications. *Kinet Catal* 53: 425–439. https://doi.org/10.1134/S0023158412040039
42. Yong GL, Chessick JJ, Hearley FH, et al. (1954) Thermodynamics of the adsorption of water on Graphon from heats of immersion and adsorption data. *J Phys Chem* 58: 313–315. https://doi.org/10.1021/j150514a006
43. Vrana LM (2014) Calcium chloride. In: *Kirk-Othmer Encyclopedia of Chemical Technology, John Wiley & Sons*. https://doi.org/10.1002/0471238961.0301120318050904.a01.pub3
44. Ng KC, Buhran M, Shahzad MW, et al. (2017) A universal isotherm model to capture adsorption uptake and energy distribution of porous heterogeneous surface. *Sci Rep* 7: 10634. https://doi.org/10.1038/s41598-017-11156-6
45. Chakraborty A, Sun B (2014) An adsorption isotherm equation for multi-types adsorption with thermodynamic correctness. *Appl Therm Eng* 72: 190–199. https://doi.org/10.1016/j.applthermaleng.2014.04.024
46. Brancato V, Frazzica A, Sapienza A, et al. (2015) Ethanol adsorption onto carbonaceous and composite adsorbents for adsorptive cooling system. *Energy* 84: 177–185. https://doi.org/10.1016/j.energy.2015.02.077

47. Liu XY, Wang WW, Xie ST, et al. (2021) Performance characterization and application of composite adsorbent LiCl@ACFF for moisture harvesting. *Sci Rep* 11: 14412. https://doi.org/10.1038/s41598-021-93784-7
48. Frazzica A, Freni A (2017) Adsorbent working pairs for solar thermal energy storage in buildings. *Renewable Energy* 110: 87–94. https://doi.org/10.1016/j.renene.2016.09.047
49. Dubinin MM, Astakhov VA (1971) Description of adsorption equilibrium of vapors on zeolites over wide ranges of temperatures and pressure. *Adv Chem* 102: 69–85. https://doi.org/10.1021/ba-1971-0102.ch044
50. Gaeini M, Rouws AL, Salari JW, et al. (2018) Characterization of microencapsulated and impregnated porous host materials based on calcium chloride for thermochemical energy storage. *Appl Energy* 212: 1165–1177. https://doi.org/10.1016/j.apenergy.2017.12.131
51. Chen Z, Zhang Y, Zhang Y, et al. (2023) A study on vermiculite-based salt mixture composite materials for low-grade thermochemical adsorption heat storage. *Energy* 278: 127986. https://doi.org/10.1016/j.energy.2023.127986
52. Fu L, Wang Q, Ye R, et al. (2017) A calcium chloride hexahydrate/ expanded perlite composite with good heat storage and insulation properties for building energy conservation. *Renew Energy* 114: 733–743. https://doi.org/10.1016/j.renene.2017.07.091
53. Liu H, Nagano K, Sugiyama D, et al. (2013) Honeycomb filters made from mesoporous composite material for an open sorption thermal energy storage system to store low-temperature industrial waste heat. *Int J Heat Mass Tran* 65: 471–480. https://doi.org/10.1016/j.ijheatmasstransfer.2013.06.021
54. Mehrabadi A, Farid M (2018) New salt hydrate composite for low-grade thermal energy storage. *Energy* 164: 194–203. https://doi.org/10.1016/j.energy.2018.08.192
55. Alsaman AS, Ibrahim EM, Askalany A, et al. (2022) Composite material-based a clay for adsorption desalination and cooling applications. *Chem Eng Res Des* 188: 417–432. https://doi.org/10.1016/j.cherd.2022.09.017
56. Kaerger J, Ruthven DM (1992) Diffusion in zeolites and other microporous solids. New York: John Wiley & Sons. https://doi.org/10.1002/apj.5500040311
57. Harned HS, Parker HW (1965) The diffusion coefficients of calcium chloride in dilute and moderately dilute solution at 25 °C. *J Am Chem Soc* 77: 265. https://doi.org/10.1021/ja01607a004
58. Valiullin RR, Skirda VD, Stapf S, et al. (1997) Molecular exchange processes in partially filled porous glass as seen with NMR diffusometry. *Phys Rev E* 55: 2664–2671. https://doi.org/10.1103/PhysRevE.55.2664
59. Zhang YN, Wang RZ, Li TX (2018) Thermochemical characterizations of high-stable activated alumina/LiCl composites with multistage sorption process for thermal storage. *Energy* 156: 240–249. https://doi.org/10.1016/j.energy.2018.05.047
60. Xu SZ, Wang RZ, Wang LW, et al. (2019) Performance characterizations and thermodynamic analysis of magnesium sulfate-impregnated zeolite 13X and activated alumina composite sorbents for thermal energy storage. *Energy* 167: 889–901. https://doi.org/10.1016/j.energy.2018.10.200
61. Pandey KM, Chaurasiya R (2017) A review on analysis and development of solar flat plate collector. *Renew Sustain Energy Rev* 67: 641–650. https://doi.org/10.1016/j.rser.2016.09.078
62. Luberti M, Gowans R, Finn P, et al. (2022) An estimate of the ultralow waste heat available in the European Union. *Energy* 238: 121967. https://doi.org/10.1016/j.energy.2021.12196

63. Scapino L, Zondag HA, Bael JV, et al. (2017) Energy density and storage capacity cost comparison of conceptual solid and liquid sorption seasonal heat storage systems for low-temperature space heating. *Renew Sustain Energy Rev* 76: 1314–1331. https://doi.org/10.1016/j.rser.2017.03.101

AIMS Press